MR 1211

AUTHORS: Livesay DE, Chen KM:

DATE: 1974

TITLE: Electromagnetic fields induced inside arbitrarily shaped biological bodies.

SOURCE: IEEE Trans Microwave Theory & Techniques MTT-22(12):1273-80

MAIN SUBJECT HEADING:

AN	HU	AT	IH	M
ANALYTICS	HUMAN EFFECTS	ANIMAL TOXICITY	WORKPLACE PRACTICES-ENGINEERING CONTROLS	MISCELLANEOUS

SECONDARY SUBJECT HEADINGS: AN HU AT IH M

- Physical/Chemical Properties
- Review
- Animal Toxicology
- Non-occupational Human Exposure
- Occupational Exposure
- Epidemiology
- Standards
- Manufacturing
- Uses
- Reactions
- Sampling/Analytical Methods
- Reported Ambient Levels
- Measured Methods
- Work Practices
- Engineering Controls
- Biological Monitoring
- Methods of Analysis
- Treatment
- Transportation/Handling/Storage/Labelling

Electromagnetic Fields Induced Inside Arbitrarily Shaped Biological Bodies

DONALD E. LIVESAY, MEMBER, IEEE, AND KUN-MU CHEN, SENIOR MEMBER, IEEE

Abstract—A theoretical method has been developed to determine the electromagnetic field induced inside heterogeneous biological bodies of irregular shapes. A tensor integral equation for the electric field inside the body was derived and solved numerically for various biological models.

I. INTRODUCTION

DURING the past few years, researchers have been engaged in a controversy over the possible hazards of nonionizing electromagnetic radiation. Humans and animals have exhibited a variety of physiological reactions to electromagnetic radiation, but investigators have been largely unable to determine whether these effects were produced thermally or nonthermally. The problem arises mainly because it is difficult to determine the electromagnetic field intensity inside an arbitrary configuration of tissues. Without knowing the field intensity, it is virtually impossible to determine the heat generation and the temperature inside the tissue structure; hence, it is difficult to judge whether the observed effect is thermal or nonthermal.

When the human body or a biological system is illuminated by an electromagnetic wave, an electromagnetic field is induced inside the body and an electromagnetic wave is scattered externally by the body. Since the human body or a biological system is an irregularly shaped heterogeneous conducting medium with frequency-dependent permittivity and conductivity, the distribution of the internal electromagnetic field and the scattered electromagnetic wave will depend on the body's physiological parameters and geometry, as well as the frequency and polarization of the incident wave.

The mathematical complexity of the problem has led researchers in this area to investigate simple models of tissue structures. Some commonly used models are the plane slab [3], [4], and the dielectric cylinder [5].

Although analyzing simple models does increase our understanding of microwave absorption and scattering by biological tissues, the results have limited applicability to arbitrary physiological systems. In our study, we have developed a general technique for calculating the electric field induced inside an arbitrary biological body by an incident electromagnetic wave. After deriving a tensor integral equation for the internal electric field, we proceeded to solve the equation numerically by the method of moments [7].

We note that Richmond [8], [9] has carried out a similar moment method solution to a two-dimensional integral equation for infinite dielectric cylinders with arbitrary cross sections. An integral-equation approach to scattering by dielectric rings has been examined by Van Doeren [10].

Manuscript received May 2, 1974; revised August 26, 1974. This work was supported in part by the National Science Foundation under Grant ENG 74-12603.

The authors are with the Department of Electrical Engineering and Systems Science, Michigan State University, East Lansing, Mich. 48824.

II. DERIVATION OF INTEGRAL EQUATION

Consider a finite body of arbitrary shape, with permittivity $\epsilon(r)$ and conductivity $\sigma(r)$, illuminated in free space by a plane electromagnetic wave as shown in Fig. 1. The induced current in the body gives rise to a scattered field E^s, which may be accounted for by replacing the body with an equivalent free-space current density J_{eq}, given by

$$J_{eq}(r) = [\sigma(r) + j\omega(\epsilon(r) - \epsilon_0)]E(r) = \tau(r)E(r). \quad (1)$$

The first term of (1) is the conduction current and the second term represents the polarization current. ϵ_0 is the free-space permittivity and $E(r)$ is the total electric field inside the body.

The scattered field inside the body may be expressed in terms of J_{eq} by using the free-space tensor Green's function $\mathsf{G}(r,r')$. However, when the field point is inside the body, E^s must be evaluated with special care because of singularity and uniqueness problems. According to Van Bladel's paper [6], the scattered field E^s at an arbitrary point inside the body can be expressed as

$$E^s(r) = \int_V J_{eq}(r') \cdot \left[\mathrm{PV}\mathsf{G}(r,r') - \frac{\mathsf{I}\delta(r-r')}{3j\omega\epsilon_0} \right] dV'$$

$$= \mathrm{PV} \int_V J_{eq}(r') \cdot \mathsf{G}(r,r')\, dV' - \frac{J_{eq}(r)}{3j\omega\epsilon_0} \quad (2)$$

where

$$\mathsf{G}(r,r') = -j\omega\mu_0 \left[\mathsf{I} + \frac{\nabla\nabla}{k_0^2} \right] \psi(r,r') \quad (3)$$

$$\psi(r,r') = \frac{\exp(-jk_0 | r - r' |)}{4\pi | r - r' |} \quad (4)$$

$$k_0 = \omega(\mu_0\epsilon_0)^{1/2}$$

μ_0 is the permeability of free space, and the PV symbol

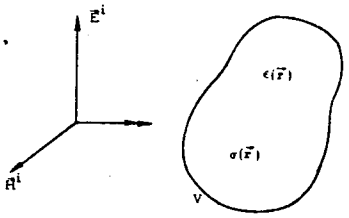

Fig. 1. An arbitrarily shaped biological body illuminated by a plane electromagnetic wave.

denotes the principal value of the integral as defined by Van Bladel [6].

We may write the total electric field $\boldsymbol{E}(r)$ inside the body as the sum of the incident electric field $\boldsymbol{E}^i$ and the scattered field $\boldsymbol{E}^s$. Thus

$$\boldsymbol{E}(r) = \boldsymbol{E}^i(r) + \boldsymbol{E}^s(r). \tag{5}$$

Substituting (2) in (5) and rearranging terms gives the desired integral equation for $\boldsymbol{E}(r)$:

$$\left[1 + \frac{\tau(r)}{3j\omega\epsilon_0}\right]\boldsymbol{E}(r) - \text{PV}\int_V \tau(r')\boldsymbol{E}(r')\cdot\mathbf{G}(r,r')\,dV' = \boldsymbol{E}^i(r). \tag{6}$$

In (6), $\boldsymbol{E}^i(r)$ is the incident electric field and is a known quantity. $\boldsymbol{E}(r)$ is the unknown total electric field inside the body. $\boldsymbol{E}(r)$ can be determined from (6) by moment methods.

III. TRANSFORMATION TO MATRIX EQUATION

We may represent the inner product $\boldsymbol{E}(r')\cdot\mathbf{G}(r,r')$ as

$$\boldsymbol{E}(r')\cdot\mathbf{G}(r,r') = \begin{bmatrix} G_{xx}(r,r') & G_{xy}(r,r') & G_{xz}(r,r') \\ G_{yx}(r,r') & G_{yy}(r,r') & G_{yz}(r,r') \\ G_{zx}(r,r') & G_{zy}(r,r') & G_{zz}(r,r') \end{bmatrix}\begin{bmatrix} E_x(r') \\ E_y(r') \\ E_z(r') \end{bmatrix}. \tag{7}$$

Let

$$x_1 = x \qquad x_2 = y \qquad x_3 = z.$$

Then, $G_{x_px_q}(r,r')$ is given by

$$G_{x_px_q}(r,r') = -j\omega\mu_0\left[\delta_{pq} + \frac{1}{k_0^2}\frac{\partial^2}{\partial x_q \partial x_p}\right]\psi(r,r'), \qquad p,q = 1,2,3. \tag{8}$$

The matrix in (7) is symmetric. Each scalar component of (6) may be written as

$$\left[1 + \frac{\tau(r)}{3j\omega\epsilon_0}\right]E_{x_p}(r) - \text{PV}\cdot\int_V \tau(r')\Big[\sum_{q=1}^{3} G_{x_px_q}(r,r')E_{x_q}(r')\Big]\,dV' = E_{x_p}{}^i(r), \qquad p = 1,2,3. \tag{9}$$

We can transform (6) into a matrix equation by using the method of moments. We partition the body into N subvolumes and assume that $E(r)$ and $\epsilon(r)$ are constants in each subvolume. We will denote the mth subvolume by V_m, and denote the position of a representative interior point of V_m by r_m. By requiring that (9) be satisfied at each r_m, we obtain, after some rearranging,

$$\left[1 + \frac{\tau(r_m)}{3j\omega\epsilon_0}\right]E_{x_p}(r_m) - \sum_{q=1}^{3}\sum_{n=1}^{N}\left[\tau(r_n)\,\text{PV}\cdot\int_{V_n} G_{x_px_q}(r_m,r')\,dV'\right]E_{x_q}(r_n) = E_{x_p}{}^i(r_m). \tag{10}$$

After defining the following quantity:

$$\tilde{G}_{x_px_q}{}^{mn} = \tau(r_n)\,\text{PV}\int_{V_n} G_{x_px_q}(r_m,r')\,dV' \tag{11}$$

we rewrite (10) as

$$\sum_{q=1}^{3}\sum_{n=1}^{N}\left[\tilde{G}_{x_px_q}{}^{mn} - \delta_{pq}\delta_{mn}\left(1 + \frac{\tau(r_m)}{3j\omega\epsilon_0}\right)\right]E_{x_q}(r_n) = -E_{x_p}{}^i(r_m), \qquad m = 1,2,\cdots,N, \quad p = 1,2,3. \tag{12}$$

Let $[G_{x_px_q}]$ be the $N \times N$ matrix whose elements are defined by

$$G_{x_px_q}{}^{mn} = \tilde{G}_{x_px_q}{}^{mn} - \delta_{pq}\delta_{mn}\left[1 + \frac{\tau(r_m)}{3j\omega\epsilon_0}\right] \tag{13}$$

and let $[E_{x_p}]$ and $[E_{x_p}{}^i]$ be N-dimensional vectors given by

$$[E_{x_p}] = \begin{bmatrix} E_{x_p}(r_1) \\ \cdot \\ \cdot \\ \cdot \\ E_{x_p}(r_N) \end{bmatrix} \qquad [E_{x_p}{}^i] = \begin{bmatrix} E_{x_p}{}^i(r_1) \\ \cdot \\ \cdot \\ \cdot \\ E_{x_p}{}^i(r_N) \end{bmatrix}, \qquad p = 1,2,3. \tag{14}$$

As m and p range over all possible values in (12), we obtain the following matrix representation of (6):

$$\left[\begin{array}{c|c|c} [G_{xx}] & [G_{xy}] & [G_{xz}] \\ \hline [G_{yx}] & [G_{yy}] & [G_{yz}] \\ \hline [G_{zx}] & [G_{zy}] & [G_{zz}] \end{array}\right]\left[\begin{array}{c} [E_x] \\ \hline [E_y] \\ \hline [E_z] \end{array}\right] = -\left[\begin{array}{c} [E_x{}^i] \\ \hline [E_y{}^i] \\ \hline [E_z{}^i] \end{array}\right]. \tag{15}$$

Symbolically, we may write (15) as

$$[G][E] = -[E^i]. \tag{16}$$

$[G]$ is a $3N \times 3N$ matrix, while $[E]$ and $[E^i]$ have dimension $3N$. We can determine the total electric field at each of the N chosen points by inverting $[G]$ in (16).

IV. EVALUATION OF MATRIX ELEMENTS

Equations (11) and (13) define the elements of $[G_{x_px_q}]$. We have

$$G_{x_px_q}{}^{mn} = \tau(r_n)\,\text{PV}\int_{V_n} G_{x_px_q}(r_m,r')\,dV' - \delta_{pq}\delta_{mn}\left[1 + \frac{\tau(r_m)}{3j\omega\epsilon_0}\right]. \tag{17}$$

Let us first consider the off-diagonal elements of $[G_{x_p x_q}]$. Clearly, $r_m \notin V_n$, so $G_{x_p x_q}(r_m,r')$ is continuous throughout V_n. Therefore, we may omit the principal value operation from our evaluation, so (17) becomes

$$G_{x_p x_q}{}^{mn} = \tau(r_n) \int_{V_n} G_{x_p x_q}(r_m,r')\, dV', \qquad m \neq n. \quad (18)$$

As a first approximation, we have

$$G_{x_p x_q}{}^{mn} = \tau(r_n) G_{x_p x_q}(r_m,r_n) \Delta V_n, \qquad m \neq n \quad (19)$$

where

$$\Delta V_n = \int_{V_n} dV'.$$

Using (8) to evaluate $G_{x_p x_q}(r_m,r_n)$ gives

$$G_{x_p x_q}{}^{mn} = \frac{-j\omega\mu_0 k_0 \tau(r_n) \Delta V_n \exp(-j\alpha_{mn})}{4\pi\alpha_{mn}{}^3} \cdot [(\alpha_{mn}{}^2 - 1 - j\alpha_{mn})\delta_{pq} + \cos\theta_{x_p}{}^{mn} \cdot \cos\theta_{x_q}{}^{mn}(3 - \alpha_{mn}{}^2 + 3j\alpha_{mn})], \qquad m \neq n \quad (20)$$

where

$$\alpha_{mn} = k_0 R_{mn} \qquad R_{mn} = |r_m - r_n|$$

$$\cos\theta_{x_p}{}^{mn} = \frac{(x_p{}^m - x_p{}^n)}{R_{mn}} \qquad \cos\theta_{x_q}{}^{mn} = \frac{(x_q{}^m - x_q{}^n)}{R_{mn}}$$

and we have written r_m and r_n as

$$r_m = (x_1{}^m, x_2{}^m, x_3{}^m) \qquad r_n = (x_1{}^n, x_2{}^n, x_3{}^n).$$

If N is sufficiently large, the approximation given by (19) and (20) may yield adequate results. For greater accuracy, (18) may be integrated numerically by any convenient method.

If the body's cross section, as seen by the incident wave, is elongated, with the longer dimension parallel to E^i, numerical integration of (18) may considerably improve the accuracy of the solution. The reason is illustrated in Fig. 2. The scattered field in subvolume V_1 contributed by a parallel unit current in subvolume V_2 has approximately twice the magnitude in Fig. 2(a) that it has in Fig. 2(b), provided $k_0 R_{12} \ll 1$, even though R_{12} is the same in both figures. In the case we are considering, most of the contributions to the scattered field are of the type shown in Fig. 2(a). Since these contributions are more significant, they should be evaluated more carefully to preserve accuracy.

For the diagonal elements of $[G_{x_p x_q}]$, (17) becomes

$$G_{x_p x_q}{}^{nn} = \tau(r_n)\ \mathrm{PV} \int_{V_n} G_{x_p x_q}(r_n,r')\, dV' - \delta_{pq}\left[1 + \frac{\tau(r_n)}{3j\omega\epsilon_0}\right]. \quad (21)$$

We approximate V_n by a sphere of equal volume centered at r_n. This enables us to evaluate the integral in (21) exactly.

Let a_n be the radius of the sphere. After a lengthy calculation (see Appendix), we find

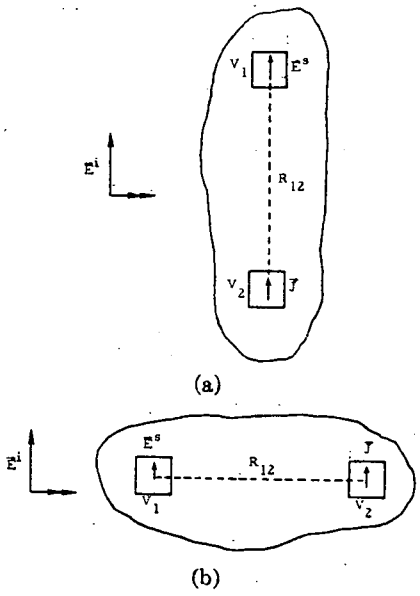

Fig. 2. (a) Scattered field in subvolume V_1 produced by unit current in subvolume V_2 when elongated body is parallel to incident field. (b) Scattered field in subvolume V_1 produced by unit current in subvolume V_2 when elongated body is perpendicular to incident field.

$$G_{x_p x_q}{}^{nn} = \delta_{pq}\left\{\frac{-2j\omega\mu_0\tau(r_n)}{3k_0{}^2}[\exp(-jk_0 a_n)(1 + jk_0 a_n) - 1] - \left[1 + \frac{\tau(r_n)}{3j\omega\epsilon_0}\right]\right\} \quad (22)$$

where

$$a_n = \left(\frac{3\Delta V_n}{4\pi}\right)^{1/3}.$$

If the actual shape of V_n differs appreciably from that of a sphere, our approximation may lead to poor numerical results. In such a case, the integration throughout a small sphere surrounding r_n can be performed as in the Appendix; the integration throughout the remainder of V_n can be done numerically.

V. SELECTED NUMERICAL RESULTS

The theory has been applied to some simple biological models. The first two examples evidence the accuracy of the numerical method.

Fig. 3 shows the electric field at the center of an electrically small dielectric cube (4 × 4 × 4 cm) illuminated by a plane wave, for various values of frequency and dielectric constant. Since the cube exhibits a symmetrical cross section to the incident wave, we only need to calculate the induced field in one quadrant, as illustrated in Fig. 3. As expected, the electric field intensity at the center of the cube is nearly equal to the electric field intensity at the center of a sphere with the same dielectric constant in a uniform electrostatic field. The field E in the sphere is given by

$$E = \left(\frac{3}{\epsilon_r + 2}\right) E^i \quad (23)$$

where E^i is the externally applied field, and $\epsilon_r = \epsilon/\epsilon_0$.

For our second example, we calculated the electric field

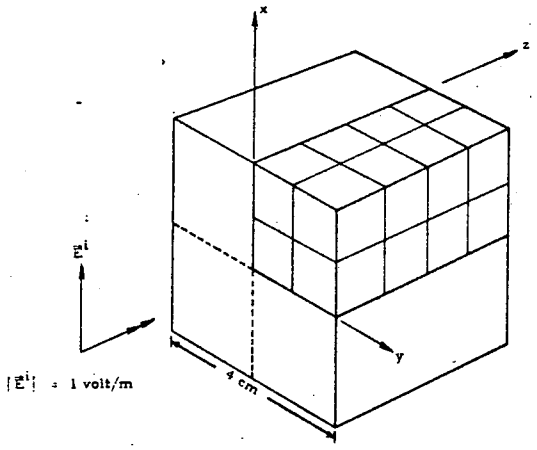

f (Hz)	λ_o (cm)	ϵ_r	λ_ϵ (cm)	$\frac{3}{\epsilon_r + 2}$	$\|\vec{E}\|$ center (volts/m)
10^7	3×10^3	5.0	1.342×10^3	0.4286	0.4172
10^6	3×10^4	5.0	1.342×10^4	0.4286	0.4172
10^3	3×10^7	5.0	1.342×10^7	0.4286	0.4172
10^3	3×10^7	20.0	6.708×10^6	0.1364	0.1124
10^3	3×10^7	51.7	4.172×10^6	0.0559	0.0503

Fig. 3. Electric field at the center of a dielectric cube (4 × 4 × 4 cm) induced by plane waves of various frequencies.

inside a thin conducting layer ($\epsilon_r = 70$, $\sigma = 1$ mho/m) illuminated by a 300-MHz plane wave. Fig. 4 shows the results when the incident electric field is perpendicular to the plane of the layer. For this case the electric field inside the layer is approximately equal to E^i/ϵ_r, consistent with the boundary conditions. If the plane of the layer is now oriented parallel to the incident electric field, the electric field inside the layer increases about ten times, as shown in Fig. 5. This example shows that the intensity of the induced electric field inside a conducting body depends heavily on the body's orientation with respect to the incident wave.

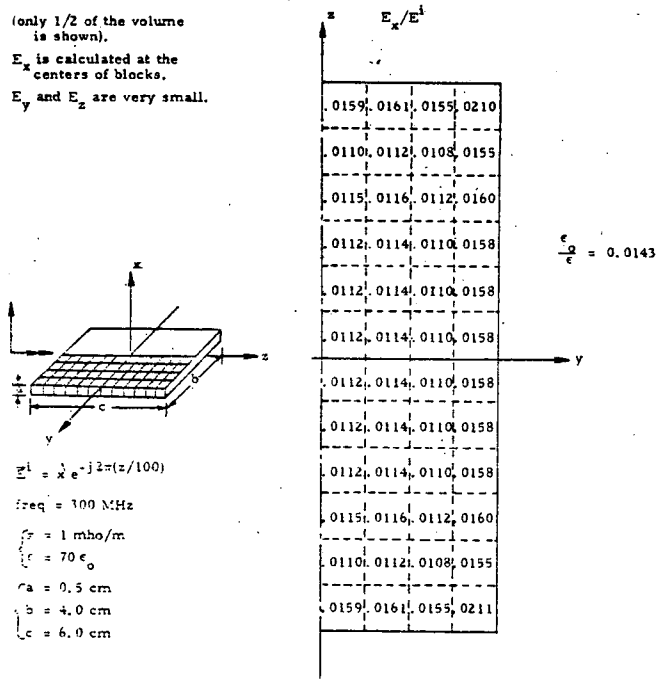

Fig. 4. Electric field inside of a layer of conducting medium with $\epsilon = 70\epsilon_0$, $\sigma = 1$ mho/m induced by a plane wave of 300 MHz with the incident electric field perpendicular to the flat surfaces of the layer.

The third example shows the induced electric field inside a tissue block (16 × 12 × 4 cm) comprising a fat layer and a muscle layer, illuminated by a 100-MHz plane wave. The distribution of the induced field is shown graphically in Fig. 6 and numerically in Fig. 7. Some interesting findings are as follows. 1) Inside the tissue block all three components of the electric field—E_x, E_y, and E_z—are induced, although the incident electric field has only an x component. We note that the induced E_z is comparable to the induced E_x in magnitude. 2) The distribution of the internal electric field is nonuniform, and its amplitude is quite different from that predicted by the plane slab model.

In the examples considered so far, the matrix elements were calculated using (20) and (22). For the remaining cases presented here, we computed the matrix elements using (22) and numerically integrating (18).

The final two examples illustrate the effects of an inhomogeneity in a thin tissue cylinder (10 cm × 1 mm × 1 mm) exposed to a 2.45-GHz plane wave. The dimensions

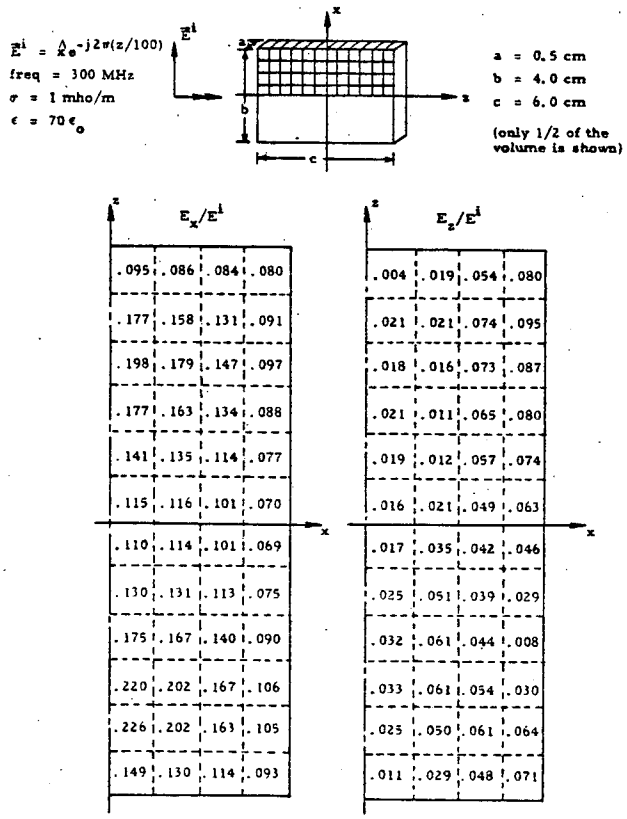

Fig. 5. Electric field inside of a layer of conducting medium with $\epsilon = 70\epsilon_0$, $\sigma = 1$ mho/m induced by a plane wave of 300 MHz with the incident electric field parallel to the flat surfaces of the layer.

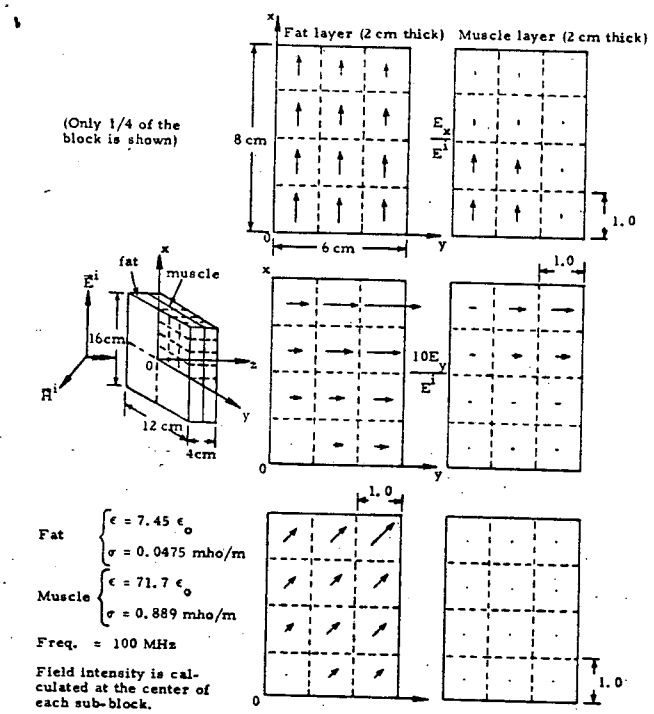

Fig. 6. Distribution of induced electric field inside of a tissue block (16 × 12 × 4 cm) consisting of a fat and a muscle layer. The incident plane wave is $E = xE^i$ with a frequency of 100 MHz. The field intensity in a corresponding infinite slab model is $E_x = 0.197E^i$ at the center of the fat layer and $E_x = 0.210E^i$ at the center of the muscle layer.

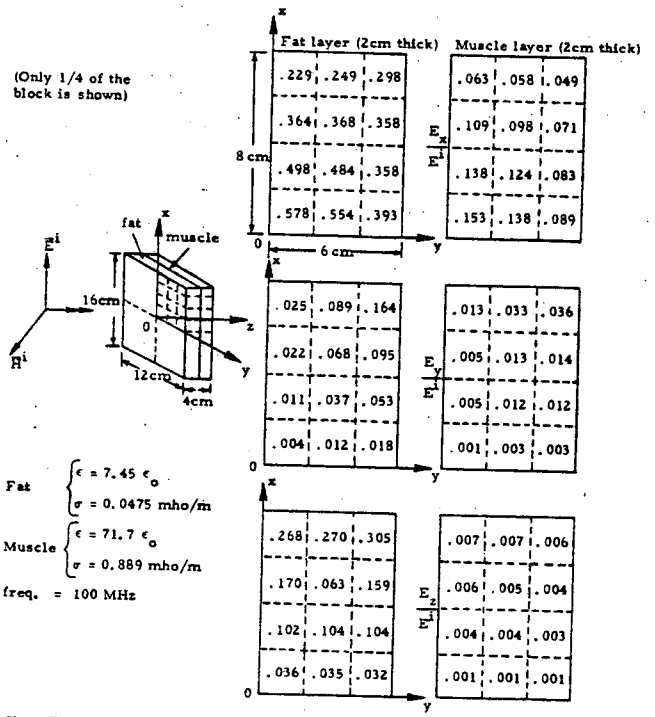

Fig. 7. Distribution of induced electric field inside of a tissue block (16 × 12 × 4 cm) consisting of a fat and a muscle layer. The field intensity is calculated at the center of each subblock. For a corresponding infinite slab model $E_x = 0.197E^i$ at the center of the fat layer and $E_x = 0.210E^i$ at the center of the muscle layer.

of the cylinder were chosen to help insure an accurate solution at this frequency. The incident electric field (x component only) is assumed to be parallel to the cylinder axis, so we may neglect the y and z components of the induced field.

Fig. 8(a) shows a homogeneous muscle cylinder, and Fig. 8(b) shows a muscle cylinder with a section of fat 1 cm long at its center. The field distribution in each cylinder is shown in Fig. 8(c), and the power density is plotted in Fig. 8(d). The discontinuity of the electric field at the muscle–fat interface in Fig. 8(c) obeys the relation

$$(\sigma_F + j\omega\epsilon_F)E_F = (\sigma_M + j\omega\epsilon_M)E_M \qquad (24)$$

where the subscripts F and M refer to fat and muscle, respectively, and E_F and E_M are both normal to the interface. Equation (24) is the boundary condition for the normal component of the electric field at the boundary of two different biological tissues.

In Fig. 9(a) we have a homogeneous fat cylinder, and in Fig. 9(b) we have a fat cylinder with a 1-cm section of muscle at its center. The distributions of the induced field and the power density are shown in Fig. 9(c) and (d), respectively. Again, the discontinuity of the electric field in Fig. 9(c) obeys (24).

From Figs. 8(d) and 9(d), we see that the inhomogeneity creates a local hot spot on the fat side of the muscle–fat boundary because the electric field is normal to the boundary. We note that in the plane slab model, the electric field is tangent to the muscle–fat interface. In that case, a local hot spot occurs in the muscle.

Of particular interest is the cylinder in Fig. 9(b). Because the muscle section is relatively small, the maximum power density occurs in the fat region. The heat generation near the center of this cylinder is several times greater than the heat generation near the center of the homogeneous cylinder of Fig. 9(a). Therefore, the temperature of an irradiated cylindrical fat structure could be significantly increased by the presence of one or more small muscle segments.

VI. DISCUSSION OF NUMERICAL RESULTS

When using a pulse function expansion in the method of moments, it is important to establish an upper limit on the dimensions of the subvolumes. To arrive at the limit for our method, we have performed two convergence tests. In both tests, the incident electric field was parallel to the x axis and had a magnitude of 1 V/m.

In the first test, we investigated a muscle cylinder, shown in Fig. 10, illuminated by a 2.45-GHz plane wave. Expressed in wavelengths, the dimensions of the cylinder were 3 × 1/2 × 1/2. Actual computations supported our assumption that the induced electric field had only an x component. We partitioned the cylinder into a variable number of cubical cells, or subvolumes, and calculated the induced field for each configuration. The models for $N = 6$, $N = 48$, and $N = 162$ are shown in Fig. 10(a)–

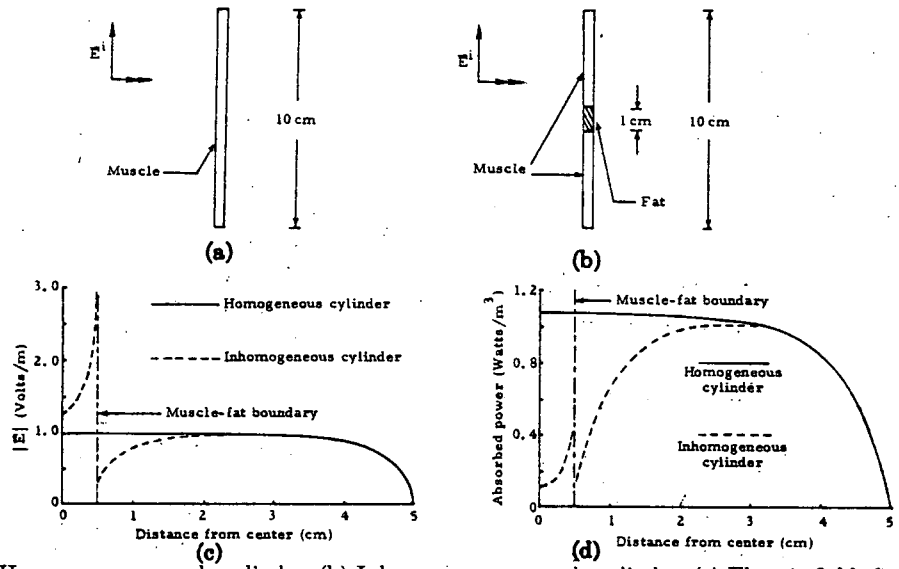

Fig. 8. (a) Homogeneous muscle cylinder. (b) Inhomogeneous muscle cylinder. (c) Electric field along cylinder axis. E^i is 1 V/m. (d) Power density $(1/2\sigma \mid E \mid^2)$ along cylinder axis. Each cylinder was partitioned lengthwise into 100 subvolumes of equal size.

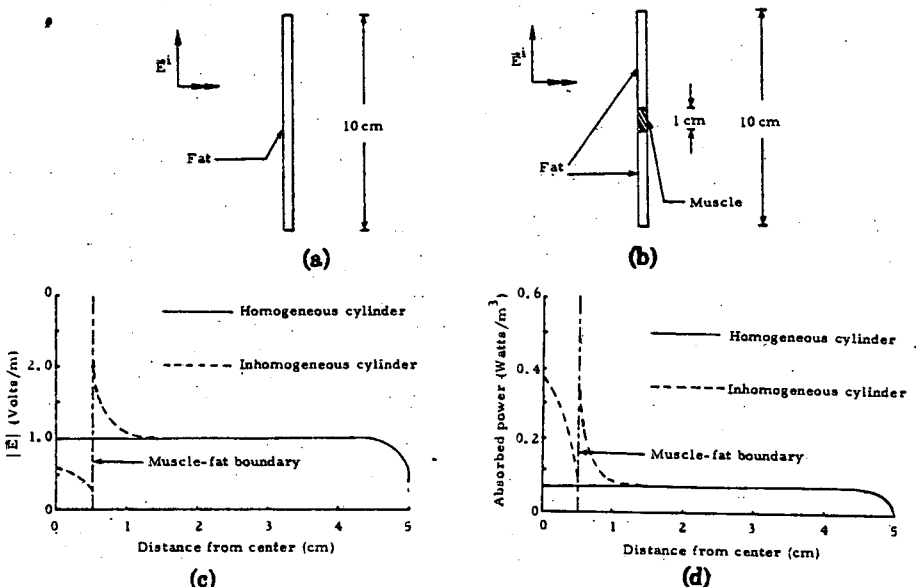

Fig. 9. (a) Homogeneous fat cylinder. (b) Inhomogeneous fat cylinder. (c) Electric field along cylinder axis. E^i is 1 V/m. (d) Power density $(1/2\sigma \mid E^2 \mid)$ along cylinder axis. Each cylinder was partitioned lengthwise into 100 subvolumes of equal size.

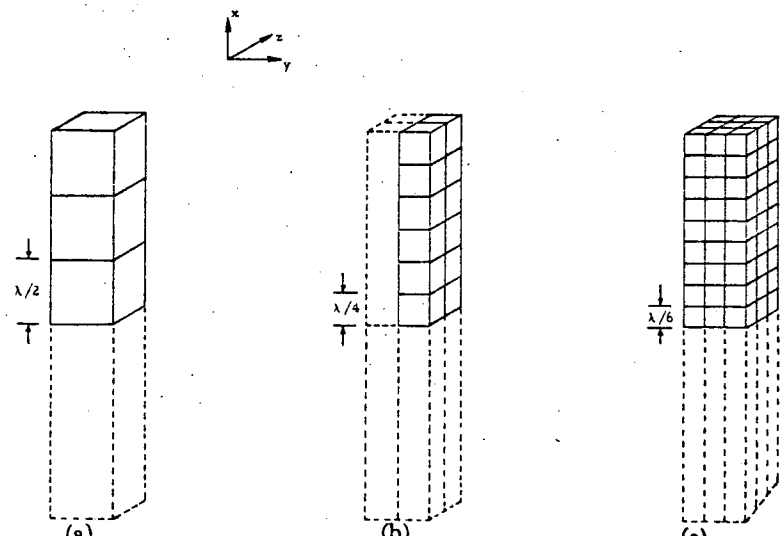

Fig. 10. A muscle cylinder illuminated by a plane wave of 2.45 GHz, partitioned into (a) 6 subvolumes, (b) 48 subvolumes, and (c) 162 subvolumes.

(c), respectively. The edges of each cell measured 1/2, 1/4, and 1/6 wavelength, respectively.

Fig. 11 shows the electric field intensity along the axis of the cylinder for each model. Since none of the subvolumes in Fig. 10(b) lie on the axis, we have plotted the average of the field intensities in the front and back of Fig. 10(b) to facilitate a comparison with Fig. 10(a) and (c). The results from all three models agree well, indicating that cells with dimensions as large as even 1/2 wavelength may produce useful data in some cases.

For the second test, we used a cube of muscle, again illuminated by a 2.45-GHz plane wave. The edges of our first sample measured one wavelength, as shown in Fig. 12(a). Treating the cube as a single cell, we calculated the induced electric field. Next, we partitioned the cube into 27 cubical subvolumes, as shown in Fig. 12(b), and again determined the induced field. We then compared the field intensity in the center cell with the value obtained from the first computation. Finally, we repeated the procedure for a 1/4-wavelength cube, shown in Fig. 12(c)

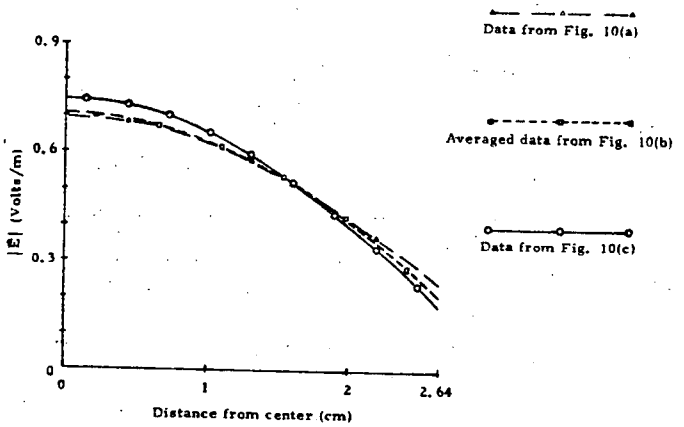

Fig. 11. Electric field intensity along the axis of the cylinder shown in Fig. 10, for models (a), (b), and (c). Frequency is 2.45 GHz. Incident field is 1 V/m. One wavelength in the cylinder is 1.76 cm.

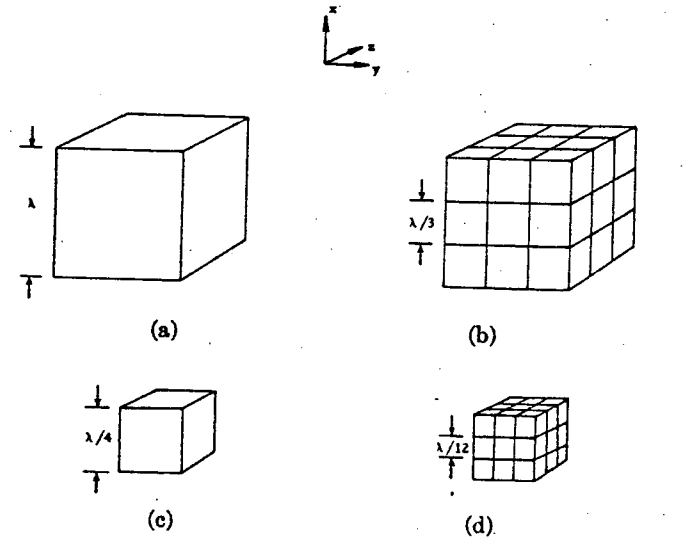

Fig. 12. Two cubes of muscle illuminated by a plane wave of 2.45 GHz, treated as single cells in (a) and (c), and partitioned into 27 subvolumes in (b) and (d). The edges of the cubes measure one wavelength and 1/4 wavelength, respectively.

TABLE I
INDUCED ELECTRIC FIELD AT THE CENTER OF THE MUSCLE CUBES SHOWN IN FIG. 12 FOR VARIOUS NUMBERS OF SUBVOLUMES

No. of cells	Size of each cell	$\|\bar{E}\|$ center (Volts/m)	Figure reference
1	λ	0.0789	12(a)
27	λ/3	0.0922	12(b)
1	λ/4	0.0592	12(c)
27	λ/12	0.0556	12(d)

Note: Frequency is 2.45 GHz; incident field is 1 V/m.

and (d). The results are given in Table I. The two values agree well for the 1/4-wavelength cube. From these results, and from those of the first test, we conclude that subvolumes having edges of 1/4 wavelength or less should yield reliable data.

Concluding our discussion of the numerical results, we note the absence of supportive experimental data from our paper. Although we have not yet verified any of our numerical data experimentally, we are now beginning a research program in which we hope to do so.

APPENDIX
EVALUATION OF MATRIX DIAGONAL ELEMENTS

In (21), let us define the following:

$$I_{x_p x_q}^{\,n} = \mathrm{PV} \int_{V_n} G_{x_p x_q}(r_n, r')\, dV'. \tag{A1}$$

As outlined in Section IV, we approximate V_n by a sphere of equal volume centered at r_n. Hence, a_n, the radius of the sphere, is given by

$$a_n = \left(\frac{3\Delta V_n}{4\pi}\right)^{1/3}. \tag{A2}$$

It is easily verified that (8) may be rewritten as

$$G_{x_p x_q}(r, r') = -j\omega\mu_0 \left[\delta_{pq} + \frac{1}{k_0^2} \frac{\partial^2}{\partial x_q' \partial x_p'}\right] \psi(r, r'). \tag{A3}$$

Since the derivatives are taken with respect to the primed variables, we are free to take $r = r_n$ at the outset. $G_{x_p x_q}(r_n, r')$ is a function of $|r_n - r'|$ only, so we may define a spherical coordinate system centered at r_n, and set $r_n = 0$. Then

$$\psi(r_n, r') = \psi(r') = \frac{\exp(-jk_0 r')}{4\pi r'} \tag{A4}$$

where

$$r' = |r'|.$$

Now

$$\frac{\partial^2 \psi}{\partial x_q' \partial x_p'} = \frac{d^2\psi}{dr'^2} \frac{x_p'}{r'} \frac{x_q'}{r'} + \frac{1}{r'} \frac{d\psi}{dr'} \left[\delta_{pq} - \frac{x_p'}{r'} \frac{x_q'}{r'}\right]. \tag{A5}$$

In our spherical coordinate system

$$x_1'/r' = \sin\theta' \cos\phi' \qquad x_2'/r' = \sin\theta' \sin\phi'$$
$$x_3'/r' = \cos\theta' \qquad dV' = r'^2 \sin\theta' \, d\theta' \, d\phi' \, dr' \tag{A6}$$

where θ' and ϕ' are the usual polar angles.

Since the primed variables are merely dummy variables, we shall omit the primes from now on. For convenience, we define the following:

$$f_{x_p x_q}(\theta,\phi) = \frac{x_p}{r}\frac{x_q}{r}. \tag{A7}$$

Equation (A1) becomes

$$I_{x_p x_q}{}^n = -j\omega\mu_0 \lim_{\eta\to 0} \int_\eta^{a_n} dr \int_0^{2\pi} d\phi \cdot \int_0^\pi \left\{ \psi\delta_{pq} + \frac{1}{k_0^2}\left[\frac{d^2\psi}{dr^2} f_{x_p x_q}(\theta,\phi) + \frac{1}{r}\frac{d\psi}{dr}\left(\delta_{pq} - f_{x_p x_q}(\theta,\phi)\right)\right]\right\} r^2 \sin\theta \, d\theta. \tag{A8}$$

Integrating by parts gives

$$I_{x_p x_q}{}^n = -j\omega\mu_0 \lim_{\eta\to 0} \left\{ \int_\eta^{a_n} dr \int_0^{2\pi} d\phi \int_0^\pi \delta_{pq}\psi r^2 \sin\theta \, d\theta + \frac{1}{k_0^2}\left(r^2 \frac{d\psi}{dr}\bigg|_\eta^{a_n}\right) \int_0^{2\pi} d\phi \int_0^\pi f_{x_p x_q}(\theta,\phi) \sin\theta \, d\theta + \frac{1}{k_0^2} \int_0^{2\pi} d\phi \int_0^\pi \left[\delta_{pq} - 3f_{x_p x_q}(\theta,\phi)\right] \sin\theta \, d\theta \cdot \int_\eta^{a_n} \frac{d\psi}{dr} r \, dr \right\}. \tag{A9}$$

In the third term of (A9),

$$\int_\eta^{a_n} \frac{d\psi}{dr} r \, dr$$

becomes infinite as $\eta \to 0$. However, it is readily verified that

$$\int_0^{2\pi} d\phi \int_0^\pi \left[\delta_{pq} - 3f_{x_p x_q}(\theta,\phi)\right] \sin\theta \, d\theta = 0, \qquad p,q = 1,2,3. \tag{A10}$$

Hence, the third term of (A9) is zero for all finite values of η, and contributes nothing as $\eta \to 0$.

It may also be readily verified that

$$\int_0^{2\pi} d\phi \int_0^\pi f_{x_p x_q}(\theta,\phi) \sin\theta \, d\theta = \frac{4\pi}{3}\delta_{pq}. \tag{A11}$$

Equation (A9) then becomes

$$I_{x_p x_q}{}^n = -j\omega\mu_0\delta_{pq} \lim_{\eta\to 0} \left\{ \int_\eta^{a_n} dr \int_0^{2\pi} d\phi \int_0^\pi \psi r^2 \sin\theta \, d\theta + \frac{4\pi}{3k_0^2} r^2 \frac{d\psi}{dr}\bigg|_\eta^{a_n} \right\}. \tag{A12}$$

After a few simple steps, we obtain

$$I_{x_p x_q}{}^n = \frac{-2j\omega\mu_0\delta_{pq}}{3k_0^2}\left[\exp\left(-jk_0a_n\right)\left(1 + jk_0a_n\right) - 1\right]. \tag{A13}$$

Substituting (A13) into (21) gives (22).

REFERENCES

[1] H. P. Schwan, "Radiation biology, medical applications, and radiation hazards," in *Microwave Power Engineering*, vol. 2, E. C. Okress, Ed. New York: Academic, 1968, pp. 215–232.

[2] J. F. Lehmann *et al.*, "Comparison of relative heating patterns produced in tissues by exposure to microwave energy at frequencies of 2450 and 900 megacycles," *Arch. Phys. Med. Rehabil.*, vol. 43, pp. 69–76, Feb. 1962.

[3] A. R. Shapiro, R. F. Lutomirski, and H. T. Yura, "Induced fields and heating within a cranial structure irradiated by an electromagnetic plane wave," *IEEE Trans. Microwave Theory Tech. (Special Issue on Biological Effects of Microwaves)*, vol. MTT-19, pp. 187–196, Feb. 1971.

[4] H. N. Kritikos and H. P. Schwan, "Hot spots generated in conducting spheres by electromagnetic waves and biological implications," *IEEE Trans. Biomed. Eng.*, vol. BME-19, pp. 53–58, Jan. 1972.

[5] H. S. Ho, A. W. Guy, R. A. Sigelmann, and J. R. Lehmann, "Electromagnetic heating patterns in circular cylindrical models of human tissue," in *Proc. 8th Annu. Conf. Medical and Biological Engineering* (Chicago, Ill.), July 1969, p. 27.

[6] J. Van Bladel, "Some remarks on Green's dyadic for infinite space," *IRE Trans. Antennas Propagat.*, vol. AP-9, pp. 563–566, Nov. 1961.

[7] R. F. Harrington, *Field Computation by Moment Methods*. New York: Macmillan, 1968, ch. 1.

[8] J. H. Richmond, "Scattering by a dielectric cylinder of arbitrary cross-section shape," *IEEE Trans. Antennas Propagat.*, vol. AP-13, pp. 334–341, May 1965.

[9] ——, "TE-wave scattering by a dielectric cylinder of arbitrary cross-section shape," *IEEE Trans. Antennas Propagat.*, vol. AP-14, pp. 460–464, July 1966.

[10] R. E. Van Doeren, "An integral equation approach to scattering by dielectric rings," *IEEE Trans. Antennas Propagat. (Communications)*, vol. AP-17, pp. 373–374, May 1969.